



## OPEN Neural representation of consciously seen and unseen information

Pablo Rodríguez-San Esteban<sup>1,2</sup>✉, Jose A. Gonzalez-Lopez<sup>3,4</sup> & Ana B. Chica<sup>1,2</sup>

Machine learning (ML) techniques have steadily gained popularity in Neuroscience research, particularly when applied to the analysis of neuroimaging data. One of the most discussed topics in this field, the neural correlates of conscious (and unconscious) information, has also benefited from these approaches. Nevertheless, further research is still necessary to better understand the minimal neural mechanisms that are necessary and sufficient for experiencing any conscious percept, and which mechanisms are comparable and discernible between conscious and unconscious events. The aim of this study was two-fold. First, to explore whether it was possible to decode task-relevant features from electroencephalography (EEG) signals, particularly those related to perceptual awareness. Secondly, to test whether this decoding could be improved by using time-frequency representations instead of voltage. We employed a perceptual task in which participants were presented with near-threshold Gabor stimuli. They were asked to discriminate the orientation of the grating, and report whether they had perceived it or not. Participants' EEG signal was recorded while performing the task and was then analysed by using ML algorithms to decode distinctive task-related parameters. Results demonstrated the feasibility of decoding the presence/absence of the stimuli from EEG data, as well as participants' subjective perception, although the model failed to extract relevant information related to the orientation of the Gabor. Unconscious processing of unseen stimulation was observed both behaviourally and at the neural level. Moreover, contrary to conscious processing, unconscious representations were less stable across time, and only observed at early perceptual stages (~100 ms) and during response preparation. Furthermore, we conducted a comparative analysis of the performance of the classifier when employing either raw voltage signals or time-frequency representations, finding a substantial improvement when the latter was used to train the model, particularly in the theta and alpha bands. These findings underscore the significant potential of ML algorithms in decoding perceptual awareness from EEG data in consciousness research tasks.

Perceptual awareness has been studied since the 1970s<sup>1</sup> to describe the cognitive processing of conscious and unconscious information<sup>2</sup>, as well as the neural correlates of conscious processing<sup>3</sup>. It has been proposed that unconscious stimuli can be either subliminal (stimuli with insufficient bottom-up strength, that cannot reach consciousness even if attended) or preconscious (stimuli with sufficient bottom-up strength, that can reach consciousness if top-down attentional amplification occurs)<sup>2,4,5</sup>. At the cognitive level, abundant evidence suggests that unconscious information is processed and affects behaviour at different processing stages<sup>6</sup>. There is, for example, evidence showing that unconscious information can be maintained in working memory<sup>7–10</sup>, can undergo semantic processing<sup>11,12</sup>, and can even be used in certain arithmetic operations<sup>13</sup>.

Despite our advanced understanding of how perceptual information is represented at various stages in the brain, a major unresolved issue in this field revolves around the debate concerning the neural representation of conscious and unconscious information. For the last decades, researchers have been trying to shed light on this conundrum by employing neuroimaging methods<sup>2,14–17</sup>, as well as studying clinical populations<sup>18–20</sup>, and using neurostimulation approaches<sup>21–24</sup>. Some authors have argued that the representation of conscious and unconscious information is similar during the early stages of processing. A large corpus of literature demonstrates that early event-related potentials (ERPs), such as the P1 and the N1, are also evoked by unseen stimuli<sup>25–28</sup>. However, around 300 ms after stimulus onset, only seen stimuli evoke components such as the

<sup>1</sup>Department of Experimental Psychology, University of Granada (UGR), Granada, Spain. <sup>2</sup>Brain, Mind, and Behavior Research Center (CIMCYC), Campus of Cartuja, University of Granada (UGR), Granada 18011, Spain. <sup>3</sup>Department of Signal Theory, Telematics and Communications, University of Granada (UGR), Granada, Spain. <sup>4</sup>Research Center for Information and Communication Technologies (CITIC-UGR), University of Granada (UGR), Granada, Spain. ✉email: prodiguez@ugr.es

P300<sup>2,28,29</sup>. More recently, this proposal has been challenged by some other authors who argue that P300 is related to post-perceptual decisional processes<sup>28,30–33</sup>. In this case, the visual awareness negativity (VAN), which can be observed at around 200 ms after stimulus onset, is proposed to be the earliest electrophysiological correlates of perceptual awareness<sup>28,31,34</sup>. It has also been claimed that the processing of unconscious representations peaks early after stimulus onset and then decays, as unconscious representations cannot be maintained for prolonged periods<sup>2,35</sup>. However, more recent data have observed that unconscious information can be preserved during relatively extended time periods<sup>36</sup>.

Focusing on the EEG literature, there is a pronounced – and growing – amount of evidence showing how brain oscillations can be interpreted as an index of conscious perception<sup>37</sup>. Specific frequency bands have been related to certain processes related to perceptual awareness, mainly alpha, beta, and gamma<sup>37</sup>. In particular, the role of gamma-band activity as a key factor in perceptual awareness remains debated<sup>37</sup>. Some authors have argued that gamma is neither exclusive to nor sufficient for conscious processing<sup>37,38</sup>, and it has been proposed that it reflects post-perceptual processes rather than access consciousness itself (in a similar fashion to the P300)<sup>32</sup>. Nevertheless, there is also an important amount of evidence that links gamma-band activity with visual awareness<sup>39,40</sup>. Oscillations in the gamma band seem to act as a synchronization mechanism, binding distributed neural activity implicated in different processes that allow conscious perception<sup>37,41</sup>. Wyart and Tallon-Baudry<sup>42</sup> explored the relationship between spatial attention and consciousness focussing on gamma modulations. They presented participants with near-threshold stimuli preceded by valid and invalid spatial cues. Results showed independent effects of consciousness and attention in different gamma bands. While consciousness modulated mid-range gamma activity, spatial attention modulated high-frequency gamma activity. This relationship between gamma-band activity and conscious perception has also been observed in multimodal studies<sup>43</sup> combining visual with auditory<sup>44</sup> and tactile<sup>45</sup> stimuli. When examining the relationship between beta-band activity and conscious perception, some studies have observed increased power<sup>46</sup> or stronger synchronization<sup>47</sup> when stimuli are consciously detected as compared to non-detected<sup>48</sup>.

The beta-band is known to be involved in the maintenance of synchronous activity across distributed brain regions. Fiebelkorn and Kastner recently proposed a rhythmic theory of attention<sup>49</sup> which proposes the existence of two alternating attentional states, one associated with increased target detection and a second one associated with decreased detection. The first state is characterized by increased activity in gamma from parietal areas and increased activity in beta from the frontal eye fields (FEF)<sup>50</sup>, supporting the associations of beta-band activity with feedback connectivity<sup>51</sup>. Increased beta has also been related to the suppression of attentional shifts and/or eye movements<sup>50</sup>. These findings link activity in the beta-band with a state of enhanced perceptual sensitivity, which then leads to an improved detection of the visual targets<sup>50</sup>. However, other studies have observed contradictory results. For example, in a study by Panagiotaropoulos et al.<sup>52</sup>, the authors investigated beta oscillations in the lateral prefrontal cortex (LPFC) of macaques during monocular physical alternation and binocular flash suppression. Their findings revealed that beta power was not significantly related to whether stimuli were consciously perceived or unconsciously suppressed. Nevertheless, the evidence against the role of beta is scarce and the literature seems to support its relationship with conscious perception<sup>53,54</sup>.

Alpha-band activity, on the other hand, has been associated with key processes for conscious perception such as spatial attention, information processing and the inhibition of distractors<sup>55–57</sup>. Increased alpha power is related to lower performance in visual perception tasks<sup>58</sup>, and pre-stimulus alpha activity can predict target detection<sup>59,60</sup>. The threshold to detect a visual stimulus has also been related to the alpha phase<sup>61</sup>. Similarly, presenting the stimuli at the peak of alpha oscillations makes them more likely to be perceived<sup>62</sup>. There is also growing evidence of the role of alpha-band activity for conscious perception using entrainment approaches, such as transcranial alternating current stimulation (tACS) and transcranial magnetic stimulation (TMS)<sup>37</sup>.

In recent years, the application of machine learning (ML) techniques, particularly in multivariate pattern analysis (MVPA), to analyze neuroimaging data has been pivotal in advancing our understanding of how information is represented in the brain. Although most prominently used in functional magnetic resonance imaging (fMRI) studies, there has been a recent increase in the application of ML techniques to analyze magnetoencephalographic and electroencephalographic (M/EEG) data (for a recent review, see<sup>63</sup>). Using these pattern classification techniques, researchers have been able to identify neural patterns related to different perceptual states. This promising methodology has, for instance, shown that expectancies induce sensory templates before stimuli are actually presented<sup>64</sup> as well as the differential patterns of activity for sensory and decision-making processes in perceptual tasks<sup>65</sup>. Clinical applications of these methods, especially in epileptic populations, have also shown promising results<sup>66</sup>.

When applied to EEG data, ML models can be trained with either voltage (either raw EEG or pre-processed epochs) or time-frequency (TF) representations. Although using voltage to train ML models has been employed in numerous studies, this approximation does not consider the role of oscillatory brain activities in cognition, which can provide valuable information about how the activity of different frequency bands is related to cognitive processes<sup>67–72</sup>. These TF representations capture both temporal and spectral dynamics simultaneously, aiding in the extraction of relevant features for understanding cognitive processes, and probably leading to improved performance in tasks like event classification and cognitive state detection. Overall, they enhance interpretability, sensitivity, and accuracy in analysing brain function and cognition. Therefore, it is possible that decoding performance could increase if the classifier is trained with TF data as compared to raw EEG. For instance, Desantis and collaborators<sup>73</sup> found that, in a visual cueing task, decoding accuracy was overall higher when fitting the model with alpha-band activity as compared to raw EEG signals.

Combining neuroimaging data with ML has yielded valuable insights into the neural representation of conscious and unconscious information. In a MEG study<sup>36</sup>, participants were asked to perform a perceptual task which consisted of detecting and shortly maintaining in working memory the orientation of a grating. The recorded signals were then fed to a ML classification model and the results showed that both the presence/absence

and the orientation (left-right) of the target stimulus could be decoded from brain activity for a prolonged period of time, even when participants did not consciously perceive the stimulus. These findings provided remarkable insight into the brain representations of visible and invisible stimuli, and how perceptual information is coded and maintained in the brain.

Following this approach, in the present study we were interested in exploring how perceptual information is represented at the neural level, and how conscious and unconscious information representation differ. We designed a perceptual task with visual preconscious stimulation, with the aim of replicating some of the findings by King and collaborators<sup>36</sup> but using EEG rather than MEG. Time-resolved decoding and temporal generalization analyses were employed, as in the MEG study, complemented with other analyses (cross-classification across blocks, decoding-behaviour correlations) to explore the differential representation of conscious and unconscious information. In addition to this, we explored whether classification accuracy would be improved when using TF data as compared to voltage, which would not only be a simple way of improving decoding scores but also provide evidence about the important role of brain oscillations for cognitive processing. Given that TF representations can capture more information about the brain dynamics, we expected that the performance of the classifiers would be improved when using this data as compared to using the voltage from the signal. When exploring specific frequency bands, based on the study by King et al.<sup>36</sup> (see time-frequency results from Fig. 50) and previous literature<sup>37</sup>, we expected that decoding performance for the task-relevant features of the stimulus (presence of the target, tilt orientation, subjective awareness) would be significantly better for the lower frequency bands, such as alpha and theta.

## Methods

The study protocol, including hypotheses, sampling plan, and analysis strategy, was pre-registered on the OSF and can be accessed at <https://osf.io/5e32h>. In addition to the analyses stated in the pre-registration, we also ran post-hoc Bayesian analyses (see Results - Cross-classification between blocks) and correlations between behavioural results and decoding scores (see Results - Post-hoc analyses: Decoding-behaviour correlations).

## Participants

Sample size calculation for decoding analysis in neuroimaging is difficult to estimate. In contrast to hypothesis-testing studies that seek to find a certain *p*-value of statistical significance, there is no standard tool for determining sample size estimates for studies using ML models such as the one presented here<sup>74–76</sup>. The difference between the two types of studies is subtle: while the former aims to find significant differences between different groups, the latter aims to obtain estimates of the predictive performance of ML models developed to validate them. For this reason, in this study we determined the sample size based on previous studies with similar approaches<sup>36,64,65,77,78</sup> which had between 20 and 25 participants, and we calculated an approximate sample size of 25 participants.

A larger sample was collected in case some participants had to be excluded from the analyses, and the final study sample included 33 volunteers (12 males, mean age 22 years, SD = 2 years). Three participants were removed from the analyses due to an insufficient number of seen targets (1 participant), at-chance accuracy for the tilt discrimination task (1 participant), and to technical issues during data recording (2 participants). Consequently, all analyses were run with a final *n* = 29. To further ensure that our sample size was sufficient for the ML analyses, we employed two strategies. First, we did a post-hoc power analysis computing the effect size of the area under the curve (AUC) metric for the classification of Target presence in TF data when compared against chance (see EEG results - Time-resolved decoding). The estimated Cohen's *d* for this case was 9.347, confirming that our sample size was adequate to detect significant differences in decoding performance. Then we performed an iterative subsampling analysis to evaluate the impact of varying the sample size on the AUC, and how the sample size influences the performance and reliability of the classification model. To do this, we ran 100 iterations for different sample sizes ranging from 5 to 29 participants, and in each iteration we computed the mean and the SD of the AUC values. What we observed was that the average AUC values remained stable at ~0.75 AUC even with smaller subsamples, and that it converged for samples with *n* > 20 participants. This approach ensured that the effects found were robust and the sample size was adequate for the performed analyses.

All participants were right-handed and had normal or corrected-to-normal vision, normal colour perception, and no prior experience with the task. No participant had a history of major medical, neurological, or psychiatric disorders. Participants received a monetary compensation of 10€/h for their participation. Signed informed consent was collected prior to their inclusion in the study. Participants were informed about their right to withdraw from the experiment at any time. The University of Granada's Ethics Committee approved the experiment (code 1862/CEIH/2020), which was carried out in accordance with the Code of Ethics of the World Medical Association (Declaration of Helsinki) for experiments involving humans.

## Apparatus and stimuli

E-Prime software version 2.0<sup>79</sup> was used for stimuli presentation and behavioural data collection. Participants were seated at an approximate distance of 70 cm from the computer screen (a 24" monitor, BenQ BL2405HT, 1920 × 1080 pixels, with a refresh rate of 60 Hz).

Trials started with a fixation display, consisting of a plus sign (0.4° × 0.4°) that appeared in the centre of the screen. The target was a Gabor stimulus generated using MATLAB 8.1 (<http://www.mathworks.com>). In total, 200 Gabor stimuli were created (spatial frequency 4 cycles/deg., 2.4° diameter, 0.1° SD) with a maximum and minimum Michelson contrast of 0.92 and 0.02, respectively. The mask consisted of a checkerboard pattern (2.4° diameter), presented largely above threshold contrast. In the tilt orientation response screen, two Gabor probes, identical to the target stimulus, were presented 0.8° above and below the fixation cross. Finally, in the Gabor

presence response screen, the words “Visto” (“Seen”, in Spanish;  $0.4^\circ \times 2^\circ$ ) and “No visto” (“Unseen”, in Spanish;  $0.4^\circ \times 3.5^\circ$ ) were displayed  $2^\circ$  above and below the fixation cross.

### Task procedure

The experiment involved three types of blocks, as depicted in Fig. 1. After an initial titration block, conducted to adjust Gabor contrast to achieve 50% seen Gabors during the experimental blocks (see description of this block below), participants performed 5 localizer blocks and 10 experimental blocks (60 trials each: 40 Gabor present and 20 Gabor absent trials), in alternating order, always starting with a localizer block followed by 2 experimental blocks. In the localizer blocks, the target was presented above threshold (around 100% seen). In the experimental blocks, target contrast was individually adjusted to achieve 50% seen trials (see below). In both localizer and experimental blocks, the target was not presented on 33.33% of the trials. The total duration of the task was approximately 75 min.

Trials in all blocks had a similar design (see Fig. 1). They started with a fixation screen, with a variable duration ranging between 1000 ms and 1500 ms. After this initial fixation, the Gabor stimulus was displayed at fixation during 50 ms, tilted clockwise or counterclockwise (with equal probability). In 33.33% of the trials, no Gabor stimulus was presented. After 300 ms, the mask was presented for 100 ms, followed by an interval of 1950 ms (ISI), in which the screen remained empty. Participants were then required to report the orientation of the lines composing the Gabor. To do this, they were presented with a clockwise-oriented Gabor, and a counterclockwise oriented Gabor, above and below the fixation cross, with the location of these stimuli being randomized across trials to avoid response preparation. This screen was presented until response. Participants responded with their right hand, pressing either the ‘k’ key associated with the stimulus above the fixation point or the ‘m’ key for the one presented below the fixation point (right hand response). Participants were asked to randomly press one of the two keys if no Gabor was perceived. Subsequently, participants were required to report the presence or absence of the Gabor, with a screen displaying the words “Seen” (“Visto”, in Spanish) and “Unseen” (“No visto”, in Spanish) above and below the fixation point, with the location of these words being also randomized across trials to avoid response preparation. This screen was displayed until a response was detected. Participants responded with their left hand, using the keys ‘d’ for the response above the fixation point and ‘c’ for the one below the fixation point. Finally, an inter-trial interval with a duration of between 1500 ms and 2000 ms was presented with the fixation cross displayed on the centre of the screen.

During the initial titration block, which was used to adjust the percentage of seen targets individually, a suprathreshold Gabor was first shown to the participants, to familiarize them with the procedure and the response keys. After this initial block, Gabor contrast was adjusted depending on participants’ performance. After every 12 trials (8 target present – 4 target absent, 4 tilted clockwise – 4 counterclockwise), if the percentage of seen stimuli exceeded 60%, the contrast was decreased in 0.5 points (in a scale of 200 different contrasts levels). Conversely, if the percentage of seen stimuli fell below 40%, the contrast was increased by 0.5 points. Once the percentage of seen targets stabilized between 60% and 40% in two consecutive blocks, the titration procedure concluded, and this contrast was used for the rest of the experimental blocks.

### EEG data acquisition

High-density EEG was acquired using an active 64-channels system mounted on a cap (actiCAP snap), an actiCHamp Plus amplifier (Brain Products GmbH, Gilching, Germany) and a computer running the BrainVision Recorder software (version 1.25.0201). Impedances were kept below 5 k $\Omega$  by applying conductive gel, following the recommendations of the amplifiers’ manufacturer, and the signal was digitized at a sampling rate of 1024 Hz. EEG activity was referenced online to the Cz electrode. Electrical activity elicited by eye movements was monitored by electro-oculogram (EOG), recorded from two electrodes (TP9-TP10) placed above and below the left eye of the participants.

### EEG analysis

#### Preprocessing

For the pre-processing and artefact detection pipeline, we selected standard procedures, similar to the ones recommended by PREP, a preprocessing pipeline for EEG analyses<sup>80</sup>, and focused on automatic procedures with the aim of applying the same steps in a future neurofeedback study. Data pre-processing was ran using MNE-Python<sup>81</sup>, and all the steps were applied on a participant-by-participant basis. First, we employed a regression-based removal of electrooculogram (EOG) artefacts implemented in MNE<sup>82,83</sup>. Next, bad channels were detected using the automatic implementation of the Random Sample Consensus (RANSAC) technique in the PyPREP

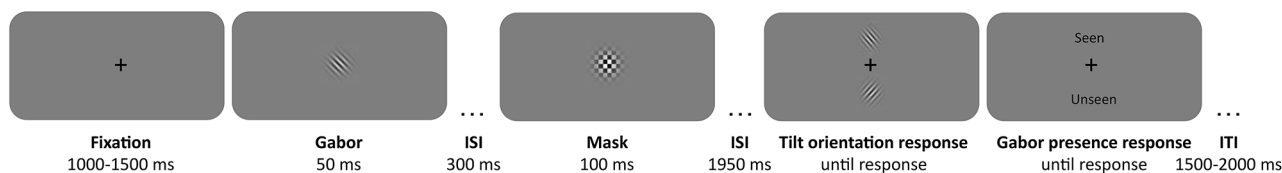


**Fig. 1.** Sequence and timing of events in a given trial. After a fixation screen of variable duration, the Gabor stimulus could be presented at the centre of the screen (no Gabor was presented in 33.33% of the trials). Participants first responded to the tilt orientation of the stimulus (clockwise or counterclockwise), and then indicated if the stimulus was seen or unseen. ISI: interstimulus interval; ITI: intertrial interval.

package<sup>84</sup>, a Python implementation of PREP<sup>80</sup>. Once the algorithm detected the bad channels in the data, these were later interpolated. Power line noise was corrected by means of a notch filter using the spectrum fit method<sup>85</sup> for the 50 Hz frequency and its two first harmonics (100 Hz and 150 Hz). Finally, the signal was re-referenced to the average of all channels.

After artefact detection and correction steps, data were segmented into epochs of  $-2000$  ms to  $+2000$  ms relative to the onset of the Gabor stimulus, applying a baseline correction from  $-200$  ms to 0. The signal was re-sampled from the original sampling rate of 1024 Hz to a frequency of 256 Hz to reduce file size and computation times. The epoched data for each participant was finally saved as “.fif” files, separately for the localizer and experimental blocks. The averaged total of epochs in the experimental blocks retained after artefact correction was 571 (95.16% of the original data, SD = 101.516).

Finally, the epoched and artifact-corrected EEG data were transformed into a time-frequency representation by using a DPSS multi-taper approach. This approach applied logarithmically spaced frequencies ranging from 4 to 50 Hz across the pre-processed epochs. An analysis window spanning 5 cycles of each frequency band was used to optimize signal representation. The TF representations of the EEG signals were computed using the MNE-Python package, specifically with the ‘tfr\_multitaper’ function and the default parameters, except the already mentioned frequencies and number of cycles.

## Decoding analyses

For the decoding analyses, the Python packages MNE<sup>81</sup> and Scikit-Learn<sup>86</sup> were used, as well as in-house adaptations of some of the code (following<sup>36</sup> and<sup>87</sup>). All the code is available at: <https://github.com/rodriguez-p/EEGConsciouslySeenUnseen>. In all the analyses, Support Vector Classification (SVC) was used to run the decoding analyses. The default parameters provided by the Scikit-Learn library were used for the SVC model, except that kernel type was set to ‘linear’ and a class-weight parameter was set to ‘balanced’ to automatically deal with the class imbalance of our data.

Time-resolved decoding analyses were run using a search light approach with the Sliding Estimator method implemented in MNE. This method fits the SVC model on each time point (or time frame of the TF features) and then evaluates the model at the same time instant but in different epochs than those used for training. This provides a time course of the decoding accuracy across all the time points of the epochs. To run the analysis, the SVC model was trained with either the epoched data (with shape  $n\_epochs, n\_channels, n\_times$ ) or the TF data ( $n\_epochs, n\_channels, n\_freqs, n\_times$ ). Since Scikit-Learn models expect 2D data ( $n\_samples, n\_features$ ), data was flattened by applying a Vectorizer, implemented in MNE, to obtain a 2D array that can be then passed to the classifier. Data was also standardized using a Standard Scaler from Scikit-Learn, which normalizes features by removing the mean and scaling to unit variance.

Additionally, a temporal generalization analysis<sup>88</sup> was run with the MNE Generalizing Estimator method. This approach is similar to the previous decoding over time analysis, but in this case the model is trained at a particular time point and then evaluated at all other time points.

Classification scores were computed with an empirical receiver operating curve (ROC) analysis and reported as the AUC and then were evaluated by using a stratified 10-fold cross-validation strategy as implemented in Scikit-Learn. This evaluation strategy randomly splits the participant data into 10 equal subsets, or *folds*, ensuring that each fold has a similar class distribution (known as *stratification*). For each iteration, the SVC model is trained on 9 folds and validated on the remaining fold. This process is repeated 10 times, rotating through all folds, so that each fold serves as the validation set once. By the end, we have 10 accuracy values, one from each fold, which can then be averaged to provide a more robust estimate of the model’s performance. This approach helps mitigate the effects of random variation in data splits and is especially useful when dealing with imbalanced datasets, as stratification ensures consistent class representation across all folds.

## Statistical testing

To assess whether the classifier performance deviated from chance (50%) and to compare accuracies between voltage and TF power, we conducted Wilcoxon signed-rank tests<sup>89</sup> on the group mean decoding performance at each time point or TF bin. The resulting p-values were then corrected for multiple comparisons by adjusting the false discovery rate (FDR)<sup>90</sup>, obtaining *q*-values (FDR adjusted p-values). This methodology aligns with previous research<sup>73,91–93</sup>.

Bayesian T-Tests were used to calculate the amount of evidence in favour of the null or the alternative hypothesis (evidence about the absence or the presence of an effect, respectively) when decoding Target presence of seen and unseen stimuli (see EEG Results - Cross-classification between blocks). For this analysis we used the Pingouin Python library<sup>94</sup> employing its default parameters, including a Cauchy scale factor of 0.707. We conducted a Bayesian T-test for each time point, comparing the results against a chance level of 0.5. The Pingouin library’s function computes the scaled Jeffrey-Zellner-Siow (JZS) Bayes Factor, which was used to evaluate the statistical evidence.

## Results

### Behavioural results

During the localizer blocks, participants reported seeing a mean of 97.4% (SD = 3%) of the presented suprathreshold Gabors and rarely caused any false alarm ( $\bar{x} = 1.9\%$ , SD = 2.4%) (Fig. 2A, left panel). During the experimental blocks, in which Gabors were presented at threshold, participants reported seeing 49% of Gabors (SD = 13.5%) and committed false alarms on 7.2% (SD = 7.3%) of the Gabor-absent trials (Fig. 2A, right panel). This result confirms that the titration procedure was successful, since the stimulus was presented at the conscious threshold and the percentage of false alarms was low. Mixed-effects linear models were fitted using the pmer4 Python package<sup>95</sup> to examine the effect of Awareness (seen, unseen) on both accuracy (ACC) and reaction times

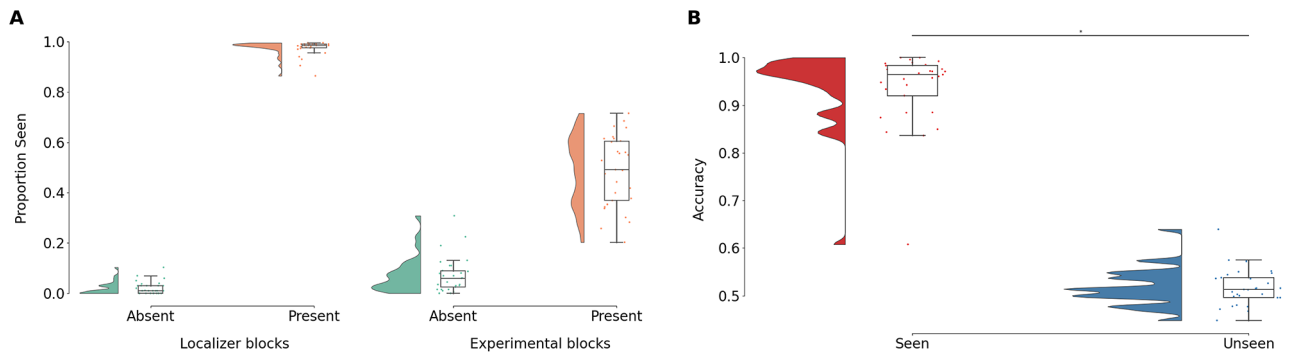


**Fig. 2.** Behavioural results. **(A)** Proportion of seen stimuli for target present and absent trials, separately for localizer and experimental blocks. **(B)** Comparison of the accuracy for seen and unseen stimuli in the experimental blocks, showing a significant effect of Awareness. Asterisks represent significant comparisons.

(RTs), accounting for individual differences through random intercepts for participants. When analysing RTs an inverse Gaussian distribution family was assumed, while for ACC the distribution was binomial. Significance of fixed effects was assessed using F-tests from the ANOVA table and p-values from the model summary. The model equations were the following:

$$\text{Accuracy} \sim \text{Awareness} + (1 \mid \text{Participant}).$$

$$\text{RT} \sim \text{Awareness} + (1 \mid \text{Participant}).$$

For ACC, participants responded more accurately to the tilt orientation task for seen ( $\bar{x} = 0.937$ ) as compared to unseen trials ( $\bar{x} = 0.523$ ) (main effect of Awareness,  $F(1, 28042.93) = 25663.77$ ,  $p < .001$ ) (Fig. 2B). Accuracy for this tilt orientation response was significantly above chance (0.5) for both seen ( $W = 435$ ,  $p < .001$ ,  $r_B = 1$ ) and unseen responses ( $W = 282.5$ ,  $p = .007$ ,  $r_B = 0.610$ ), as reported by a Wilcoxon one sample signed-rank test. This indicates that when participants were able to see the stimulus, they reported the Gabor orientation almost perfectly, and their responses were slightly above chance when they could not see the Gabor. For RTs, participants' responses were faster for unseen ( $\bar{x} = 646$  ms) as compared to seen responses ( $\bar{x} = 922$  ms) (main effect of Awareness,  $F(1, 28037.62) = 1248.53$ ,  $p < .001$ ).

## EEG results

### Time-resolved decoding

To explore brain representations of Target presence (present vs. absent), Awareness (seen vs. unseen) and Gabor orientation (left vs. right) across time, we conducted a time-resolved analysis aimed at determining the decoding performance of the ML model across the whole epoch. This analysis was run on voltage data (the pre-processed epochs; Fig. 3A) and on TF power (Fig. 3B).

In the experimental blocks (in which approximately 50% of the targets were seen), we first compared the model's performance against chance along the entire time window, fitting the model with voltage data to decode Target presence, Awareness, and Gabor orientation. Decoding scores for Target presence and Awareness were significantly different from chance starting at approximately 200 ms after target presentation until the end of the epoch ( $q < 0.001$ ), as can be observed in Fig. 3. When exploring the effect of Gabor tilt, no significant differences were found ( $q > 0.001$ ). To test if the lack of accurate decoding of the tilt information was due to the weak strength of the Gabor stimulus, we ran the same model with data from the localizer blocks, in which the grating was presented above-threshold. Similar results were obtained, with no significant differences from chance ( $q > 0.001$ ; see Supplementary material, Figure S1A). In a post-hoc analysis, instead of extracting data from the complete set of electrodes, we selected a subset of posterior channels following the procedure of a previous study by Wolff et al.<sup>96</sup>. Again, decoding scores did not reach significance ( $q > 0.001$ , Figure S1B). This suggests that, with the current task and using EEG data, it is not possible to accurately classify the orientation of the Gabor stimulus.

When using TF power to fit the ML model (Fig. 3B), Target presence and Awareness decoding scores were significantly different from chance starting at approximately 100 ms after target presentation until the end of the epoch ( $q < 0.001$ ). In contrast, decoding performance for Gabor tilt was not different from chance at any time point ( $q > 0.001$ ).

Since we were interested in evaluating whether the decoding analyses were improved by using TF representations, we conducted direct comparisons for the decoding scores when using voltage against the scores for TF power in the three experimental conditions (see Fig. 4). For Target presence, scores for TF power were significantly higher than voltage decoding scores. In the case of Awareness, decoding performance for TF power was greater than for voltage after target presentation. Again, for Gabor tilt, no significant differences were found, as performance for both TF power and voltage oscillating was around chance level (Fig. 4C).

Since better decoding scores were obtained from TF EEG representations, in the rest of this document we only used those representations for our analyses.

### Time-frequency decoding

To explore the role of specific brain oscillations in brain representations, we used TF decoding (see Fig. 5A). This approach is similar to the temporal decoding method, but instead of only examining the temporal course

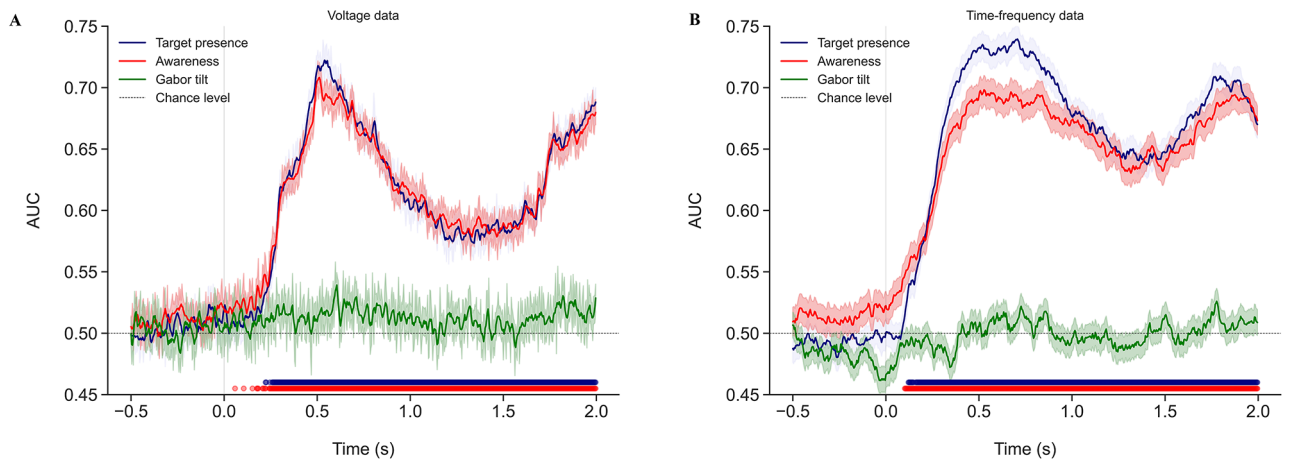


**Fig. 3.** Temporal decoding performance for (A) voltage data and (B) time-frequency (TF) power data. The x-axis represents time (in seconds) relative to the onset of the Gabor presentation ( $t=0$ ), and the y-axis shows the area under the curve (AUC) as a measure of decoding accuracy. The horizontal dashed line indicates chance-level performance ( $AUC=0.5$ ). Colored lines represent decoding accuracy for Target presence (blue), Awareness (red), and Gabor tilt (green), with shaded regions showing the mean  $\pm$  the standard error of the mean (SEM) across participants. Significant differences from chance are marked by colored dots along the x-axis ( $q < 0.001$ ), indicating robust decoding for Target presence and Awareness shortly after the Gabor presentation and persisting until the end of the epoch. In contrast, decoding accuracy for Gabor tilt remains close to chance, suggesting that this feature was not reliably decoded.

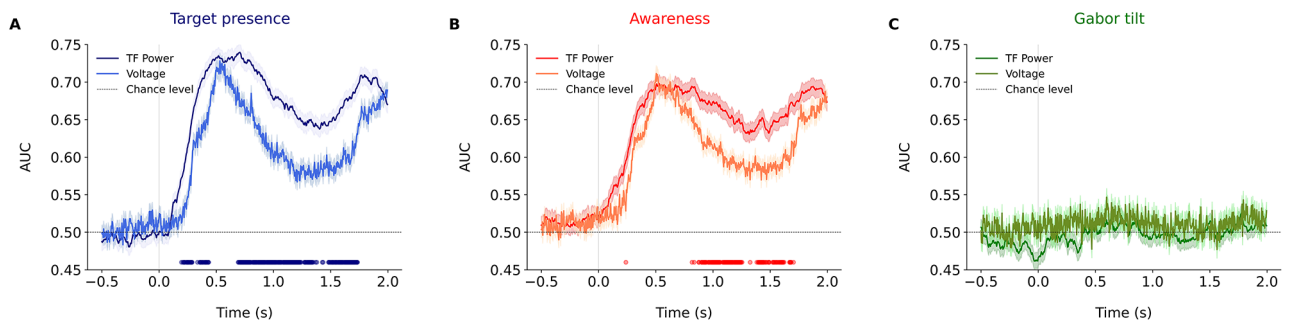


**Fig. 4.** Temporal decoding performance comparing voltage and time-frequency (TF) power features for (A) Target presence, (B) Awareness, and (C) Gabor tilt. The x-axis represents time (in seconds) relative to the Gabor presentation ( $t=0$ ), and the y-axis shows the area under the curve (AUC) as a measure of decoding accuracy. The horizontal dashed line indicates chance-level performance ( $AUC=0.5$ ). Colored lines and shaded regions represent the mean  $\pm$  SEM across participants for each condition. Significant differences from chance ( $q < 0.001$ ) are marked by dots along the x-axis. Robust decoding performance was observed for Target presence and Awareness in both voltage and TF power domains. For Target presence, the differences appear shortly after Gabor presentation and are maintained for a prolonged period, disappearing before the end of the epoch. For Awareness, significant differences are found at a later time window in the trial, between  $\sim 800$ ms and  $\sim 1600$ ms. In contrast, decoding performance for Gabor tilt remained at chance level throughout the epoch.

of the decoding scores, the data is segregated by TF time frame (see Methods). For both Target presence and Awareness, greater than chance AUC scores could be found between 4 Hz and 30 Hz, with the highest values for the theta and alpha frequency bands (see Fig. 5B). Again, for Gabor tilt, no comparisons against chance reached significance ( $q > 0.001$ ).

### Generalization across time

We also employed a Temporal Generalization method to examine how the patterns of the neural activity in our data generalized across different time points. This analysis examines the dynamics of neural representations over time, showing how a specific pattern of activity evolves across distinct time points<sup>88</sup>. The diagonal points represent the traditional measure of decoding accuracy where the classifier is trained and tested at the same time point (as in the time-resolved analysis of Fig. 3), and the off-diagonal points indicate the generalization of the

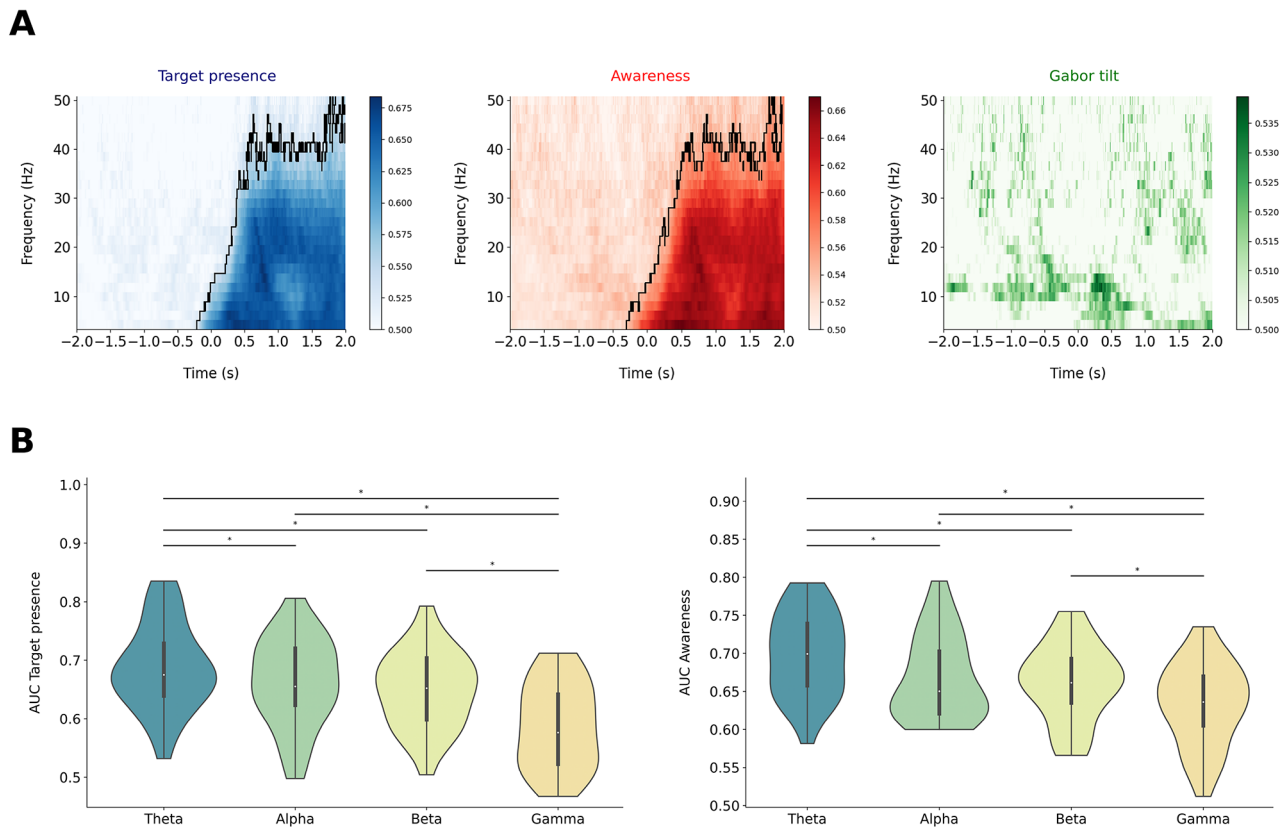


**Fig. 5.** Model performance for the TF data. **(A)** Decoding scores segregated by TF bins. Higher decoding accuracy was found from Gabor onset ( $t=0$ ) between 5 and 30 Hz, for both Target presence (top-left panel) and Awareness (top-middle panel), but not for Gabor tilt (top-right panel). Black contour lines indicate TF bins where decoding performance was significantly different from chance ( $q < 0.001$ ). The colorbar on the right represents the mean AUC. **(B)** Violin plots representing the statistical distribution of decoding scores for each frequency band. Best overall results are obtained when using the theta band, which has the highest mean AUC for both Target presence (bottom-left panel) and Awareness (bottom-right panel). Asterisks represent significant comparisons among frequency bands.

activity patterns across different time points. Significant decoding during prolonged periods is interpreted as evidence for sustained cognitive processes.

For both Target presence and Awareness, greater than chance performance was found during the entire epoch ( $q < 0.001$ ). High AUC scores can be observed in the diagonal of the matrix, i.e. where training and testing data come from the same time points. When looking at off-diagonal elements, two sustained processes can be observed with an early peak around 200 ms and 800 ms after target presentation, and a late process at the end of the epoch around 1500 ms and 2000 ms. When analysing Gabor tilt, no significant differences were found ( $q > 0.001$ ) (Fig. 6).

### Cross-classification between blocks

To explore how seen and unseen stimuli were differentially represented in the brain, we first trained the ML model on the Localizer blocks (in which targets were highly visible) and later evaluated it on the Experimental blocks (where only 50% of the targets were consciously seen) separately for seen and unseen trials. The main question to be responded to with this analysis was: Can we decode Target presence even if participants did not consciously perceive the stimulus during the experimental blocks? Temporal generalization matrices showed significant differences for seen (Fig. 7B) but not for unseen (Fig. 7C) trials. For seen stimuli, an earlier sustained process can be observed from approximately 200ms to 800ms after target onset, and a later process around 1700ms.

When analysing decoding accuracies across time (Fig. 7A), for seen trials, decoding scores were significantly different from chance ( $q < 0.001$ ) right after the presentation of the stimuli and until the end of the trial. However, for unseen trials, no significant differences were found. To further explore this null result, we ran post-hoc analyses using Bayesian analyses for seen and unseen trials, comparing the classifier performance against chance (0.5) for each time point. Results demonstrated strong and consistent evidence in favour of the alternative hypothesis for the seen trials from Gabor onset until the end of the epoch. For the unseen trials, however, there were some time points in which evidence in favour of the alternative hypothesis was found. Decoding scores were slightly different from chance in two time windows: an early time window right after target onset (~100

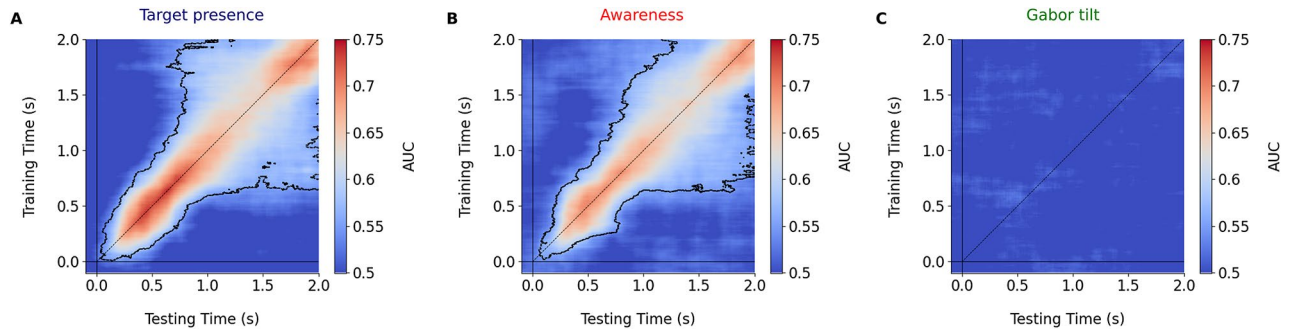


**Fig. 6.** Temporal generalization matrices for decoding performance across time for (A) Target presence, (B) Awareness, and (C) Gabor tilt. Each matrix shows the decoding scores (area under the curve, AUC) for all pairwise combinations of training and testing time points, with the x-axis representing training time and the y-axis representing testing time relative to the Gabor presentation ( $t=0$ ). Significant decoding scores ( $q < 0.001$ ) are outlined with black contour lines. Robust generalization was observed for Target presence and Awareness, with significant decoding extending from the Gabor presentation to the end of the epoch, indicating consistent temporal patterns across training and testing windows. In contrast, no significant decoding was observed for Gabor tilt, suggesting a lack of discriminative temporal information for this feature.

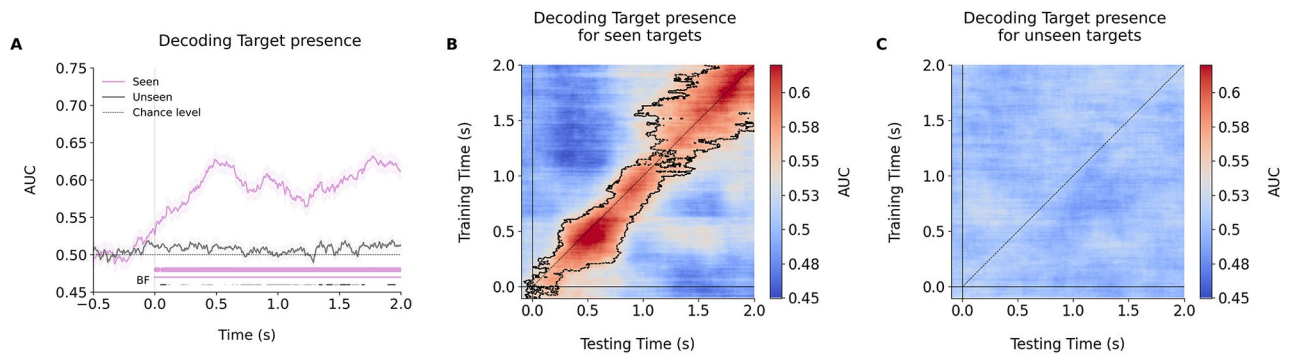


**Fig. 7.** Cross-classification decoding performance for seen and unseen stimuli. (A) Time-resolved analysis: The x-axis represents time relative to the Gabor presentation ( $t=0$ ), and the y-axis shows decoding accuracy (area under the curve, AUC). Significant differences from chance ( $q < 0.001$ ) for seen trials are indicated by thick pink dots above the x-axis, starting shortly after stimulus presentation and persisting until the end of the epoch. No significant differences were found for unseen trials using frequentist statistics. Bayesian analysis results are shown as thinner dots, with light pink (seen) and grey (unseen) colors indicating  $BF < 0.33$  (evidence for the null hypothesis) and darker colors indicating  $BF > 3$  (evidence for the alternative hypothesis). Shaded regions represent mean  $\pm$  SEM across participants. (B-C) Temporal generalization matrices for seen (B) and unseen (C) trials. Each matrix depicts decoding performance across training (x-axis) and testing (y-axis) time points. Significant decoding scores ( $q < 0.001$ ) for seen trials are outlined with black contour lines, demonstrating robust temporal generalization. No significant decoding scores were observed for unseen trials.

ms) and a later time window (with some significant values starting from  $\sim 1300$  ms until the end of the epoch). In most parts of the epoch, Bayesian analysis showed evidence in favour of the null hypothesis, indicating that Target presence was not represented consistently for a prolonged period of time. This analysis demonstrates evidence of unconscious processing although only in a few, discrete time points at early (perceptual) and late (response preparation) stages of processing.

In order to further explore unconscious representations, we run all previous analyses separately for a set of posterior electrodes and for a set of anterior electrodes. The results were similar to those found when using all the channels. In the frequentist analyses, we found no significant decoding for unseen stimuli in either set of electrodes (see Supplementary material, Fig S5). With the Bayesian analyses, we observed evidence in favour of the null hypothesis in most of the time window for unseen trials, although there were some time points in which we observed evidence in favour of the alternative hypothesis. In the anterior set of channels, the only significant evidence in favour of the alternative hypothesis was found at around 900 ms after Gabor onset, and then at around 1700 ms, i.e. at the end of the trial (Figure S5A). This roughly corresponds with the late decoding peak we found with the complete set of electrodes (Fig. 7A), which could be related to response preparation processes. In the posterior electrodes, we observed an early significant time point after Gabor onset, similar to the one presented in Fig. 7A, and some other significant time points between  $\sim 500$  ms and 1500 ms (Figure

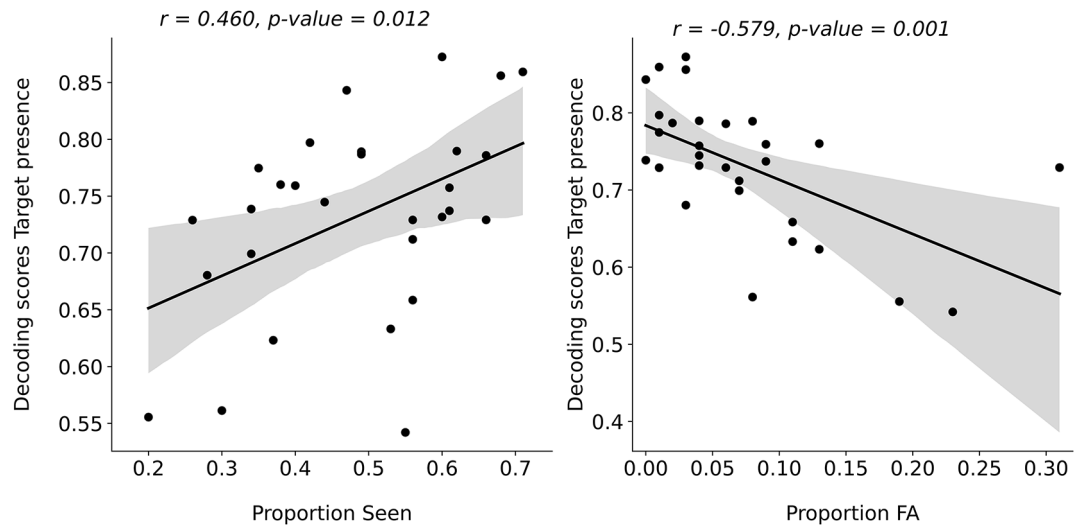


**Fig. 8.** Pearson correlations between decoding accuracy for Target presence and the proportion of seen targets in target present trials (left panel) and the proportion of false alarms in target absent trials (right panel). The black line represents the best fit of the data and the shaded area represents the 95% CI for the regression estimate.

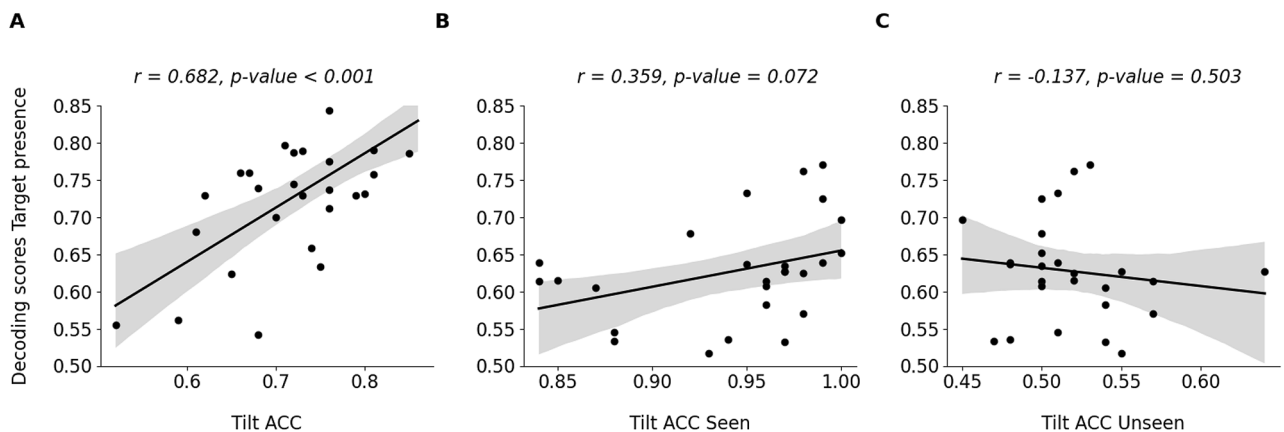


**Fig. 9.** Pearson correlation between decoding accuracy for Target presence and the accuracy in the tilt discrimination task for the overall ACC (A) and separately for seen (B) and unseen (C) trials. The black line represents the best fit of the data and the shaded area represents the 95% CI for the regression estimate.

S5D). However, note that Bayesian analyses were not planned and were only run a posteriori, so these findings should be interpreted carefully.

#### **Post-hoc analyses: Decoding-behaviour correlations.**

To explore whether neural representations were related to participants' performance, we carried out some decoding-behaviour correlations. Firstly, we explored whether perceptual representations of Target presence improved for those participants with better detection performance (i.e., an increased percentage of seen targets in target present trials, or a decreased percentage of false alarms in target absent trials). Figure 8 shows that this is the case, as decoding accuracy for Target presence was significantly correlated both with the proportion of seen targets ( $r = .46, p = .012$ ) and false alarms ( $r = -.59, p = .001$ ).

Then, we analysed if decoding accuracy of target presence was also related with the accuracy of the tilt discrimination task, where we also found significant correlations between the decoding performance for Target presence and tilt discrimination accuracy ( $r = .61, p < .001$ ; Fig. 9A). When the correlation was separately performed for seen and unseen trials, we found that although not statistically significant, there was a clear trend for a correlation between Target presence decoding accuracy and performance in the tilt discrimination task for seen trials ( $r = .36, p = .07$ ), but not for unseen trials ( $r = -.14, p = .50$ ) (Fig. 9B and C). This is an important result in relation to the brain representation of conscious and unconscious stimuli. For consciously perceived stimuli, the brain representation of Target presence could be enhanced for those participants with better performance in the tilt discrimination task. However, for unseen stimuli, the neural representation of Target presence was not different in participants with different accuracies in the tilt response task (which ranged between 45 and 65%).

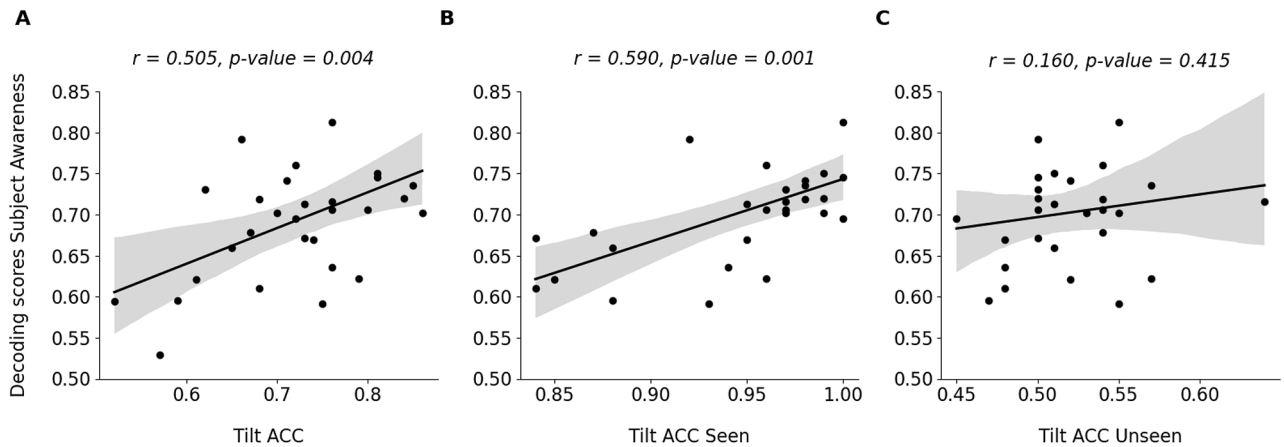


**Fig. 10.** Pearson correlation between decoding accuracy for Awareness and the ACC in the tilt discrimination task, for the overall ACC (A) and separately for seen (B) and unseen (C) trials. The black line represents the best fit of the data, and the shaded area represents the 95% CI for the regression estimate.

We then explored whether the overall decoding accuracy of Awareness was related with the behavioural accuracy in the tilt discrimination task. As shown in Fig. 10A, this was the case. When the correlation was separately performed for seen and unseen trials, we observed a significant correlation for seen trials ( $r = .59$ ,  $p = .001$ , Fig. 10B), but not for unseen trials ( $r = .16$ ,  $p = .41$ , Fig. 10C).

Finally, and given the evidence of unconscious processing observed when decoding Target presence for unseen trials (see Fig. 7), we planned some post-hoc analyses to explore the nature of the unconscious representation observed. If the decoding of Target presence in early time windows (which was mostly observed in posterior channels) was related to perceptual processes, then decoding accuracy during this time window could correlate with the behavioural accuracy in the tilt discrimination task. Moreover, if the decoding of Target presence in late time window ( $> 1500$  ms, which was mostly observed in anterior channels) was related to response preparation, then decoding accuracy during this time window could correlate with the overall RT. To test for this post-hoc hypotheses, we correlated the decoding scores of Target presence for early and late time windows with the overall tilt accuracy, and tilt accuracy for seen and unseen trials, as well as with the overall RT, and RT for seen and unseen trials (see Supplementary material, Figures S6 and S7). For the early time window, none of the correlations were significant. However, for the late time window, there was a significant correlation between the decoding of Target presence and the RT for unseen trials. Higher decoding scores during late time windows were related to faster RTs. This result confirms our prediction that the representation of unconscious stimuli during late time windows was related to an increased motor response preparation at the end of the trial.

## Discussion

The aim of this study was to explore conscious and unconscious information representations at a neural level. We used EEG to decode Target presence, Awareness, and tilt orientation, comparing decoding accuracies of raw EEG signal and TF data. Participants were required to perform a detection and discrimination task with preconscious near-threshold Gabor patches. In a localizer block, Gabors were presented above-threshold ( $\sim 100\%$  seen), while in the experimental blocks, target contrast was titrated to achieve  $\sim 50\%$  seen targets. On 33.33% of the trials, no Gabor was presented. We analyzed the registered signal using ML, specifically classification analyses, to observe if the decoder would be able to categorize different task features from the EEG data. We found that the classifier had significantly higher than chance performance when classifying Target presence and Awareness, but not Gabor tilt. Although Gabor tilt has been successfully decoded using magnetoencephalography (MEG)<sup>36,97–99</sup>, this information seems not to be decodable in any of the analysis carried out in this EEG study.

An important debate in the field of the neuroscience of consciousness is related to the existence of unconscious processing of unseen stimuli. In the previously mentioned study by King et al.<sup>36</sup>, they used ML applied to MEG data and found that (1) participants responded above chance in the tilt discrimination task when the stimulus was unseen, and (2) target presence could be decoded for seen but also for unseen stimuli. In our data, behavioural evidence of unconscious processing was also found, as tilt responses were slightly above chance for unseen stimuli. To explore the neural representation of unseen stimuli, we trained a ML classifier to decode the Target presence on trials with supra-threshold stimuli (in the localizer blocks) and then tested it with near-threshold stimuli (perceived on  $\sim 50\%$  of the trials, in the experimental block), separately for seen and unseen trials. As expected, strong and consistent decoding was observed for Target presence in seen trials. For unseen trials, the representation of Target presence did not reach statistical significance when using frequentist analysis. However, when using Bayesian statistics to test for the null effect, we observed that although in most of the analysed window there was evidence against the null hypothesis (i.e. we had evidence of absence of neural representation of Target presence for unseen stimuli), there were some discrete windows in which there was evidence in favour of the alternative hypothesis. These two windows roughly corresponded with the two sustained processes observed in seen trials in the Temporal Generalization analysis (see Fig. 6). Target

presence could be briefly decoded for unseen stimuli in an early time window (~100 ms after Gabor onset) and a late one (with some significant results from ~1300ms until the end of the trial). Neural representations at early time windows for unconscious information have been previously reported<sup>2,25–27,36</sup> and indicate that the initial stages of processing in sensory modules are preserved for unconscious information<sup>2,4</sup>. This representation was not maintained during the trial, as there were numerous moments in which there was evidence in favour of the null hypothesis. This is also consistent with the proposal that unconscious information cannot be maintained for long periods<sup>2,35</sup> (but see also<sup>36</sup>). In fact, at the end of the trial, where participants could predict that the response display will soon be presented, there were some discrete moments in which Target presence could again be decoded. This could indicate that, even if the target remained unconscious, there could be some information in the system about its presence that allowed participants to prepare themselves for responding. Accordingly, for unseen trials, decoding accuracies of Target presence were associated with RTs. This interesting result indicates that, even if the target did not reach consciousness, unconscious representations can prepare the system to respond faster although not better (as there was no correlation with tilt accuracy). It should be noted that Bayesian analyses were run a posteriori and not initially planned, so these findings should be interpreted with caution. Further research would benefit from the application of Bayesian statistics in the study of conscious perception with EEG data and decoding approaches.

A further aim of the present study was to examine whether decoding accuracy could be improved by using TF signal representations instead of raw EEG voltage. Our results showed that decoding scores were significantly improved when using TF power as compared to voltage for Target presence and Awareness, but Gabor tilt could not be decoded neither with raw voltage nor with TF. This result adds to the literature demonstrating that TF data provides rich information about how certain cognitive processes are represented in the brain<sup>100–102</sup>. It also suggests that when using EEG, performance of classifiers can be improved by adding an additional step to the analysis pipeline to transform the pre-processed data to obtain TF representations. Traditional approaches have used raw EEG or ERPs, but these measures are unable to capture all the information encoded in the EEG signal. For example, ERP methods assume temporal consistency of the component across trials, prioritizing neural activity that is time-locked to the event of interest and disregarding any non-phase-locked signals<sup>103–105</sup>. Meanwhile, when using TF methods, we can characterize the EEG signal as oscillatory activity and capture different aspects of this signal such as its amplitude, frequency and phase<sup>104,106,107</sup>. Combining these measures provides information on how the amplitude and phase of these neural oscillations change over time, and across different frequency bands<sup>106</sup>. Oscillatory activity is a fundamental property of the brain<sup>101,108,109</sup>, providing more direct insights into the neurophysiological mechanisms underlying the cognitive processes captured by the EEG data. As such, TF representations are relevant in the study of other biosignals, such as speech, where TF representations are used for the recognition of spoken words and phrases in modern automatic speech recognition (ASR) systems<sup>110,111</sup>.

More specifically, when exploring decoding performance across different frequency bands, we found significantly higher scores in the lower-frequency bands, particularly in theta (4–7 Hz) and alpha (7–12 Hz), both for the classification of Target Presence and Awareness. There exists a vast literature reporting associations between the theta and alpha bands with different cognitive processes<sup>112,113</sup>, including attention and memory<sup>56,114–117</sup>. When looking specifically at the evidence of studies dealing with visual perception and awareness, alpha has been commonly related to these processes<sup>60–62,118,119</sup> and changes in the power and/or amplitude of this band have been proposed as one of the neural correlates of consciousness. In a study by Bareither and collaborators<sup>120</sup>, participants were presented with subliminal and supraliminal visual stimuli. They found that alpha activity was different for visible and invisible stimuli, with an enhanced alpha decrease for visible than invisible stimuli. Modulations of post-stimulus alpha power have also been reported in a number of studies<sup>121,122</sup>, even in more recently developed no-report paradigms<sup>123</sup>, as well as in neuromodulation studies<sup>124</sup>. Taken altogether, this evidence points to a critical role of alpha-band activity in perceptual awareness. As for the importance of theta-band activity on our decoding results, one possible explanation could be related to its association with ERPs. There is substantial evidence supporting the relationship between theta activity and some ERP components, especially with the P3<sup>125–128</sup> but also others such as the N2 and the error-related negativity<sup>127,129</sup>. These findings suggest that lower frequency bands such as theta and delta represent processes underlying ERPs, being able to capture these slower components of the EEG signal that can be misrepresented when doing time-frequency analyses.

Decoding performance was also significantly higher than chance for beta, although accuracy of the classification was significantly lower than that of theta and alpha. Beta-band activity has been traditionally related to sensorimotor processing, although its role in cognitive processes is still a matter of debate and study<sup>100</sup>. In this regard, some studies have found evidence for a role of beta-band activity in the maintenance of the current cognitive set<sup>100</sup> and top-down control in tasks involving, for example, motion perception<sup>130</sup>. An interesting line of research has also observed important modulations on the power of alpha/beta power in relation with a number of different cognitive processes including memory and perception<sup>131</sup>, in the form of task-dependent power decreases. Finally, although gamma-band activity had the smallest contribution to decoding accuracies in our task, in the last years large evidence has emerged demonstrating an important role of these oscillations in multiple cognitive processes such as attention, memory, multisensory processing and perceptual awareness<sup>43,100,132,133</sup>.

## Conclusions

Our study demonstrates that neural representation of the presence/absence of a visual stimulus and its subjective perception can be reliably decoded from EEG signals. Decomposing the signals into the time-frequency domain significantly enhances decoding performance, with slow frequency bands – particularly the theta band – contributing most prominently to the decoding performance (theta > (alpha = beta) > gamma). Furthermore,

our findings reveal that conscious representations are robust and temporarily consistent, whereas unconscious representations, though detectable at both early and late stages of processing, are weaker and more inconsistent over time. Correlations with behavior suggest that unconscious representations may facilitate faster responses, but they do not improve response accuracy. These results provide new insights into the neural dynamics underlying conscious and unconscious visual processing and their behavioral implications.

### Data availability

Raw EEG data can be found at the following OpenNeuro repository: <https://openneuro.org/datasets/ds005273>. Behavioural data and task files can be accessed at: <http://osf.io/rgk8w>.

Received: 22 June 2024; Accepted: 27 February 2025

Published online: 06 March 2025

### References

- Raffone, A., Srinivasan, N. & Van Leeuwen, C. Perceptual awareness and its neural basis: bridging experimental and theoretical paradigms. *Philos. Trans. R. Soc. B Biol. Sci.* **369**, 20130203 (2014).
- Dehaene, S. & Changeux, J.-P. Experimental and Theoretical Approaches to Conscious Processing. *Neuron* **70**, 200–227 (2011).
- Koch, C., Massimini, M., Boly, M. & Tononi, G. Neural correlates of consciousness: progress and problems. *Nat. Rev. Neurosci.* **17**, 307–321 (2016).
- Dehaene, S., Changeux, J.-P., Naccache, L., Sackur, J. & Sergent, C. Conscious, preconscious, and subliminal processing: a testable taxonomy. *Trends Cogn. Sci.* **10**, 204–211 (2006).
- Kanai, R., Walsh, V. & Tseng, C. Subjective discriminability of invisibility: A framework for distinguishing perceptual and attentional failures of awareness. *Conscious. Cogn.* **19**, 1045–1057 (2010).
- Dresp-Langley, B. Why the brain knows more than we do: non-conscious representations and their role in the construction of conscious experience. *Brain Sci.* **2**, 1–21 (2011).
- Gambarota, F., Tsuchiya, N., Pastore, M., Di Polito, N. & Sessa, P. Unconscious visual working memory: A critical review and Bayesian meta-analysis. *Neurosci. Biobehav. Rev.* **136**, 104618 (2022).
- Bergström, F. & Eriksson, J. Neural evidence for non-conscious working memory. *Cereb. Cortex* **28**, 3217–3228 (2018).
- Bergström, F. & Eriksson, J. The conjunction of non-consciously perceived object identity and spatial position can be retained during a visual short-term memory task. *Front. Psychol.* **6**, (2015).
- Soto, D., Mäntylä, T. & Silvanto, J. Working memory without consciousness. *Curr. Biol.* **21**, R912–R913 (2011).
- Kiefer, M. Top-down modulation of unconscious ‘automatic’ processes: A gating framework. *Adv. Cogn. Psychol.* **3**, 289–306 (2008).
- Naccache, L. Conscious influences on subliminal cognition exist and are asymmetrical: Validation of a double prediction. *Conscious. Cogn.* **17**, 1359–1360 (2008).
- Karpinski, A., Briggs, J. C. & Yale, M. A direct replication: Unconscious arithmetic processing. *Eur. J. Soc. Psychol.* **49**, 637–644 (2019).
- Dellert, T. *et al.* Dissociating the neural correlates of consciousness and task relevance in face perception using simultaneous EEG-fMRI. *J. Neurosci.* **41**, 7864–7875 (2021).
- Friedman, G., Turk, K. W. & Budson, A. E. The current of consciousness: Neural correlates and clinical aspects. *Curr. Neurol. Neurosci. Rep.* **23**, 345–352 (2023).
- Kronemer, S. I. *et al.* Human visual consciousness involves large scale cortical and subcortical networks independent of task report and eye movement activity. *Nat. Commun.* **13**, 7342 (2022).
- Nani, A. *et al.* The neural correlates of consciousness and attention: Two sister processes of the brain. *Front. Neurosci.* **13**, 1169 (2019).
- Colás, I. *et al.* Conscious perception in patients with prefrontal damage. *Neuropsychologia* **129**, 284–293 (2019).
- Farah, M. & Feinberg, T. Consciousness of perception after brain damage. *Semin. Neurol.* **17**, 145–152 (1997).
- Mazzi, C., Mazzeo, G. & Savazzi, S. Markers of TMS-evoked visual conscious experience in a patient with altitudinal hemianopia. *Conscious. Cogn.* **54**, 143–154 (2017).
- Bachmann, T. On a strategy of advancement of TMS based methods for studying NCC. *Front. Psychol.* **9**, 2026 (2018).
- De Graaf, T. A. & Sack, A. T. Using brain stimulation to disentangle neural correlates of conscious vision. *Front. Psychol.* **5**, (2014).
- Koenig, L. & Ro, T. Dissociations of conscious and unconscious perception in TMS-induced blindsight. *Neuropsychologia* **128**, 215–222 (2019).
- Mattavelli, G. *et al.* TMS-EEG approach unveils brain mechanisms underlying conscious and unconscious face perception. *Brain Stimulat.* **12**, 1010–1019 (2019).
- Sergent, C., Baillet, S. & Dehaene, S. Timing of the brain events underlying access to consciousness during the attentional blink. *Nat. Neurosci.* **8**, 1391–1400 (2005).
- Marti, S. & Dehaene, S. Discrete and continuous mechanisms of temporal selection in rapid visual streams. *Nat. Commun.* **8**, 1955 (2017).
- Marti, S., King, J.-R. & Dehaene, S. Time-resolved decoding of two processing chains during dual-task interference. *Neuron* **88**, 1297–1307 (2015).
- Mashour, G. A., Roelfsema, P., Changeux, J.-P. & Dehaene, S. Conscious processing and the global neuronal workspace hypothesis. *Neuron* **105**, 776–798 (2020).
- Charles, L., King, J.-R. & Dehaene, S. Decoding the dynamics of action, intention, and error detection for conscious and subliminal stimuli. *J. Neurosci.* **34**, 1158–1170 (2014).
- Andersen, L. M., Pedersen, M. N., Sandberg, K. & Overgaard, M. Occipital MEG activity in the early time range (<300 ms) predicts graded changes in perceptual consciousness. *Cereb. Cortex* **26**, 2677–2688 (2016).
- Koivisto, M. & Grassini, S. Neural processing around 200 ms after stimulus-onset correlates with subjective visual awareness. *Neuropsychologia* **84**, 235–243 (2016).
- Pitts, M. A., Padwal, J., Fennelly, D., Martínez, A. & Hillyard, S. A. Gamma band activity and the P3 reflect post-perceptual processes, not visual awareness. *NeuroImage* **101**, 337–350 (2014).
- Ye, M. & Lyu, Y. Later positivity reflects post-perceptual processes: Evidence from immediate detection and delayed detection tasks. *Front. Psychol.* **10**, 82 (2019).
- Eklund, R. & Wiens, S. Visual awareness negativity is an early neural correlate of awareness: A preregistered study with two Gabor sizes. *Cogn. Affect. Behav. Neurosci.* **18**, 176–188 (2018).
- Kiefer, M. & Spitzer, M. Time course of conscious and unconscious semantic brain activation. *NeuroReport* **11**, (2000).
- King, J.-R., Pescetelli, N. & Dehaene, S. Brain mechanisms underlying the brief maintenance of seen and unseen sensory information. *Neuron* **92**, 1122–1134 (2016).

37. Gallotto, S., Sack, A. T., Schuhmann, T. & De Graaf, T. A. Oscillatory correlates of visual consciousness. *Front. Psychol.* **8**, 1147 (2017).
38. Luo, Q. *et al.* Visual awareness, emotion, and gamma band synchronization. *Cereb. Cortex* **19**, 1896–1904 (2009).
39. Meador, K. J., Ray, P. G., Echaiz, J. R., Loring, D. W. & Vachtsevanos, G. J. Gamma coherence and conscious perception. *Neurology* **59**, 847–854 (2002).
40. Zhang, Z. *et al.* Early High-gamma activity in human visual cortex increases with visual awareness. *J. Vis.* **22**, 4452 (2022).
41. Engel, A. K. & Singer, W. Temporal binding and the neural correlates of sensory awareness. *Trends Cogn. Sci.* **5**, 16–25 (2001).
42. Wyart, V. & Tallon-Baudry, C. Neural dissociation between visual awareness and spatial attention. *J. Neurosci.* **28**, 2667–2679 (2008).
43. Senkowski, D., Schneider, T. R., Foxe, J. J. & Engel, A. K. Crossmodal binding through neural coherence: implications for multisensory processing. *Trends Neurosci.* **31**, 401–409 (2008).
44. Balz, J. *et al.* GABA concentration in superior temporal sulcus predicts gamma power and perception in the sound-induced flash illusion. *NeuroImage* **125**, 724–730 (2016).
45. Lange, J., Oostenveld, R. & Fries, P. Perception of the touch-induced visual double-flash illusion correlates with changes of rhythmic neuronal activity in human visual and somatosensory areas. *NeuroImage* **54**, 1395–1405 (2011).
46. Gross, J. *et al.* Modulation of long-range neural synchrony reflects temporal limitations of visual attention in humans. *Proc. Natl. Acad. Sci.* **101**, 13050–13055 (2004).
47. Gaillard, R. *et al.* Converging intracranial markers of conscious access. *PLoS Biol.* **7**, e1000061 (2009).
48. Haque, H., Lobier, M., Palva, J. M. & Palva, S. Neuronal correlates of full and partial visual conscious perception. *Conscious. Cogn.* **78**, 102863 (2020).
49. Fiebelkorn, I. C. & Kastner, S. A rhythmic theory of attention. *Trends Cogn. Sci.* **23**, 87–101 (2019).
50. Fiebelkorn, I. C. & Kastner, S. Functional specialization in the attention network. *Annu. Rev. Psychol.* **71**, 221–249 (2020).
51. Bastos, A. M. *et al.* Visual areas exert feedforward and feedback influences through distinct frequency channels. *Neuron* **85**, 390–401 (2015).
52. Panagiotaropoulos, T. I., Kapoor, V. & Logothetis, N. K. Desynchronization and rebound of beta oscillations during conscious and unconscious local neuronal processing in the macaque lateral prefrontal cortex. *Front. Psychol.* **4**, (2013).
53. Koenig, L. & He, B. J. Spontaneous slow cortical potentials and brain oscillations independently influence conscious visual perception. *PLoS Biol.* **23**, e3002964 (2025).
54. Vernet, M., Stengel, C., Quentin, R., Amengual, J. L. & Valero-Cabré, A. Entrainment of local synchrony reveals a causal role for high-beta right frontal oscillations in human visual consciousness. *Sci. Rep.* **9**, 14510 (2019).
55. Klimesch, W., Sauseng, P. & Hanslmayr, S. EEG alpha oscillations: The inhibition–timing hypothesis. *Brain Res. Rev.* **53**, 63–88 (2007).
56. Klimesch, W. Alpha-band oscillations, attention, and controlled access to stored information. *Trends Cogn. Sci.* **16**, 606–617 (2012).
57. Capilla, A., Schoffelen, J.-M., Paterson, G., Thut, G. & Gross, J. Dissociated  $\alpha$ -band modulations in the dorsal and ventral visual pathways in visuospatial attention and perception. *Cereb. Cortex* **24**, 550–561 (2014).
58. Hanslmayr, S. *et al.* Visual discrimination performance is related to decreased alpha amplitude but increased phase locking. *Neurosci. Lett.* **375**, 64–68 (2005).
59. Ergenoglu, T. *et al.* Alpha rhythm of the EEG modulates visual detection performance in humans. *Cogn. Brain Res.* **20**, 376–383 (2004).
60. Van Dijk, H., Schoffelen, J.-M., Oostenveld, R. & Jensen, O. Prestimulus oscillatory activity in the alpha band predicts visual discrimination ability. *J. Neurosci.* **28**, 1816–1823 (2008).
61. Busch, N. A., Dubois, J. & VanRullen, R. The phase of ongoing EEG oscillations predicts visual perception. *J. Neurosci.* **29**, 7869–7876 (2009).
62. Mathewson, K. E., Gratton, G., Fabiani, M., Beck, D. M. & Ro, T. To see or not to see: prestimulus  $\alpha$  phase predicts visual awareness. *J. Neurosci.* **29**, 2725–2732 (2009).
63. Saeidi, M. *et al.* Neural decoding of EEG signals with machine learning: A systematic review. *Brain Sci.* **11**, 1525 (2021).
64. Kok, P., Mostert, P. & de Lange, F. P. Prior expectations induce prestimulus sensory templates. *Proc. Natl. Acad. Sci.* **114**, 10473–10478 (2017).
65. Mostert, P., Kok, P. & de Lange, F. P. Dissociating sensory from decision processes in human perceptual decision making. *Sci. Rep.* **5**, 18253 (2016).
66. Rasheed, K. *et al.* Machine learning for predicting epileptic seizures using EEG signals: A review. *IEEE Rev. Biomed. Eng.* **14**, 139–155 (2021).
67. Başar, E., Başar-Eroglu, C., Karakaş, S. & Schürmann, M. Gamma, alpha, delta, and theta oscillations govern cognitive processes. *Int. J. Psychophysiol.* **39**, 241–248 (2001).
68. Harmony, T. The functional significance of delta oscillations in cognitive processing. *Front. Integr. Neurosci.* **7**, (2013).
69. Kahana, M. J. The cognitive correlates of human brain oscillations. *J. Neurosci.* **26**, 1669–1672 (2006).
70. Mazaheri, A., Slagter, H. A., Thut, G. & Foxe, J. J. Orchestration of brain oscillations: principles and functions. *Eur. J. Neurosci.* **48**, 2385–2388 (2018).
71. Sauseng, P. & Klimesch, W. What does phase information of oscillatory brain activity tell us about cognitive processes? *Neurosci. Biobehav. Rev.* **32**, 1001–1013 (2008).
72. Ward, L. M. Synchronous neural oscillations and cognitive processes. *Trends Cogn. Sci.* **7**, 553–559 (2003).
73. Desantis, A., Chan-Hon-Tong, A., Collins, T., Hogendoorn, H. & Cavanagh, P. Decoding the temporal dynamics of covert spatial attention using multivariate EEG analysis: Contributions of raw amplitude and alpha power. *Front. Hum. Neurosci.* **14**, 570419 (2020).
74. Balki, I. *et al.* Sample-Size Determination methodologies for machine learning in medical imaging research: A systematic review. *Can. Assoc. Radiol. J.* **70**, 344–353 (2019).
75. Flint, C. *et al.* Systematic misestimation of machine learning performance in neuroimaging studies of depression. *Neuropsychopharmacology* **46**, 1510–1517 (2021).
76. Goldenholz, D. M., Sun, H., Ganglberger, W. & Westover, M. B. Sample size analysis for machine learning clinical validation studies. *Biomedicines* **11**, 685 (2023).
77. Bae, G.-Y. & Chen, K.-W. EEG decoding reveals task-dependent recoding of sensory information in working memory. *NeuroImage* **297**, 120710 (2024).
78. Kaiser, D., Stecher, R. & Doerschner, K. EEG decoding reveals neural predictions for naturalistic material behaviors. *J. Neurosci.* **43**, 5406–5413 (2023).
79. Schneider, W., Eschman, A. & Zuccolotto, A. *E-Prime 2.0*. (Psychology Software Tools, Inc, Pittsburgh, 2002).
80. Bigdely-Shamlo, N., Mullen, T., Kothe, C., Su, K.-M. & Robbins, K. A. The PREP pipeline: Standardized preprocessing for large-scale EEG analysis. *Front. Neuroinformatics* **9**, (2015).
81. Gramfort, A. MEG and EEG data analysis with MNE-Python. *Front. Neurosci.* **7**, (2013).
82. Croft, R. J. & Barry, R. J. Removal of ocular artifact from the EEG: A review. *Neurophysiol. Clin. Neurophysiol.* **30**, 5–19 (2000).
83. Gratton, G., Coles, M. G. H. & Donchin, E. A new method for off-line removal of ocular artifact. *Electroencephalogr. Clin. Neurophysiol.* **55**, 468–484 (1983).

84. Appelhoff, S. *et al.* PyPREP: A Python implementation of the preprocessing pipeline (PREP) for EEG data. (2022) doi:10.5281/ZENODO.6363576.
85. Mitra, P. & Bokil, H. *Observed Brain Dynamics*. (Oxford University Press, Oxford ; New York, 2008).
86. Pedregosa, F. *et al.* Scikit-learn: Machine learning in python. *J. Mach. Learn. Res.* **12**, 2825–2830 (2011).
87. Gennari, G., Dehaene, S., Valera, C. & Dehaene-Lambertz, G. Spontaneous supra-modal encoding of number in the infant brain. *Curr. Biol.* **33**, 1906–1915.e6 (2023).
88. King, J.-R. & Dehaene, S. Characterizing the dynamics of mental representations: the temporal generalization method. *Trends Cogn. Sci.* **18**, 203–210 (2014).
89. Wilcoxon, F. Individual comparisons by ranking methods. *Biom. Bull.* **1**, 80 (1945).
90. Benjamini, Y. & Hochberg, Y. Controlling the false discovery rate: A practical and powerful approach to multiple testing. *J. R. Stat. Soc. Ser. B Methodol.* **57**, 289–300 (1995).
91. Correia, J. M., Jansma, B., Hausfeld, L., Kikkert, S. & Bonte, M. EEG decoding of spoken words in bilingual listeners: from words to language invariant semantic-conceptual representations. *Front. Psychol.* **6**, (2015).
92. Grootswagers, T., Wardle, S. G. & Carlson, T. A. Decoding dynamic brain patterns from evoked responses: A tutorial on multivariate pattern analysis applied to time series neuroimaging data. *J. Cogn. Neurosci.* **29**, 677–697 (2017).
93. Jaeger, M., Mirkovic, B., Bleichner, M. G. & Debener, S. Decoding the attended speaker from EEG using adaptive evaluation intervals captures fluctuations in attentional listening. *Front. Neurosci.* **14**, 603 (2020).
94. Vallat, R. Pingouin: Statistics in Python. *J. Open Source Softw.* **3**, 1026 (2018).
95. Jolly, E. Pymer4: Connecting R and python for linear mixed modeling. *J. Open Source Softw.* **3**, 862 (2018).
96. Wolff, M. J., Ding, J., Myers, N. E. & Stokes, M. G. Revealing hidden states in visual working memory using electroencephalography. *Front. Syst. Neurosci.* **9**, (2015).
97. Allen, H., Murai, Y., Manassi, M., Amano, K. & Whitney, D. Decoding the orientation of small targets in the periphery using magnetoencephalography. *J. Vis.* **21**, 2723 (2021).
98. Pantazis, D. *et al.* Decoding the orientation of contrast edges from MEG evoked and induced responses. *NeuroImage* **180**, 267–279 (2018).
99. Ramkumar, P., Jas, M., Pannasch, S., Hari, R. & Parkkonen, L. Feature-specific information processing precedes concerted activation in human visual cortex. *J. Neurosci.* **33**, 7691–7699 (2013).
100. Engel, A. K. & Fries, P. Beta-band oscillations — signalling the status quo? *Curr. Opin. Neurobiol.* **20**, 156–165 (2010).
101. Buzsáki, G. & Draguhn, A. Neuronal oscillations in cortical networks. *Science* **304**, 1926–1929 (2004).
102. Fries, P. A mechanism for cognitive dynamics: Neuronal communication through neuronal coherence. *Trends Cogn. Sci.* **9**, 474–480 (2005).
103. Morales, S. *et al.* Time–frequency dynamics of error monitoring in childhood: An EEG study. *Dev. Psychobiol.* **64**, e22215 (2022).
104. Morales, S. & Bowers, M. E. Time-frequency analysis methods and their application in developmental EEG data. *Dev. Cogn. Neurosci.* **54**, 101067 (2022).
105. Luck, S. J. *An Introduction to the Event-Related Potential Technique*. (MIT Press, 2014).
106. Cohen, M. X. *Analyzing Neural Time Series Data: Theory and Practice*. (MIT Press, 2014).
107. Cohen, M. X. A better way to define and describe Morlet wavelets for time-frequency analysis. *NeuroImage* **199**, 81–86 (2019).
108. Doelling, K. B. & Assaneo, M. F. Neural oscillations are a start toward understanding brain activity rather than the end. *PLOS Biol.* **19**, e3001234 (2021).
109. Beste, C., Münchau, A. & Frings, C. Towards a systematization of brain oscillatory activity in actions. *Commun. Biol.* **6**, 137 (2023).
110. Ayvaz, U. *et al.* Automatic speaker recognition using mel-frequency cepstral coefficients through machine learning. *Comput. Mater. Contin.* **71**, 5511–5521 (2022).
111. Toledano, D. T., Fernández-Gallego, M. P. & Lozano-Diez, A. Multi-resolution speech analysis for automatic speech recognition using deep neural networks: Experiments on TIMIT. *PLOS ONE* **13**, e0205355 (2018).
112. Benwell, C. S. Y. *et al.* Prestimulus EEG power predicts conscious awareness but not objective visual performance. *eneuro* **4**, ENEURO.0182-17.2017 (2017).
113. Chaumon, M. & Busch, N. A. Prestimulus neural oscillations inhibit visual perception via modulation of response gain. *J. Cogn. Neurosci.* **26**, 2514–2529 (2014).
114. Busch, N. A. & VanRullen, R. Spontaneous EEG oscillations reveal periodic sampling of visual attention. *Proc. Natl. Acad. Sci.* **107**, 16048–16053 (2010).
115. Cavanagh, J. F., Cohen, M. X. & Allen, J. J. B. Prelude to and resolution of an error: EEG phase synchrony reveals cognitive control dynamics during action monitoring. *J. Neurosci.* **29**, 98–105 (2009).
116. Klimesch, W. EEG alpha and theta oscillations reflect cognitive and memory performance: a review and analysis. *Brain Res. Rev.* **29**, 169–195 (1999).
117. Ostrowski, J. & Rose, M. Increases in pre-stimulus theta and alpha oscillations precede successful encoding of crossmodal associations. *Sci. Rep.* **14**, 7895 (2024).
118. Hutchinson, B. T., Pammer, K. & Jack, B. Pre-stimulus alpha predicts inattention blindness. *Conscious. Cogn.* **87**, 103034 (2021).
119. Zazio, A., Ruhnau, P., Weisz, N. & Wutz, A. Pre-stimulus alpha-band power and phase fluctuations originate from different neural sources and exert distinct impact on stimulus-evoked responses. *Eur. J. Neurosci.* **55**, 3178–3190 (2022).
120. Bareither, I., Chaumon, M., Bernasconi, F., Villringer, A. & Busch, N. A. Invisible visual stimuli elicit increases in alpha-band power. *J. Neurophysiol.* **112**, 1082–1090 (2014).
121. Babiloni, C., Vecchio, F., Bultrini, A., Luca Romani, G. & Rossini, P. M. Pre- and Poststimulus alpha rhythms are related to conscious visual perception: A high-resolution EEG study. *Cereb. Cortex* **16**, 1690–1700 (2005).
122. Cobos, M. I., Melcón, M., Rodríguez-San Esteban, P., Capilla, A. & Chica, A. B. The role of brain oscillations in feature integration. *Psychophysiology* **61**, e14467 (2024).
123. Harris, A. M., Dux, P. E. & Mattingley, J. B. Awareness is related to reduced post-stimulus alpha power: a no-report inattention blindness study. *Eur. J. Neurosci.* **52**, 4411–4422 (2020).
124. Romei, V., Gross, J. & Thut, G. On the role of prestimulus alpha rhythms over occipito-parietal areas in visual input regulation: Correlation or causation? *J. Neurosci.* **30**, 8692–8697 (2010).
125. Başar, E., Başar-Eroğlu, C., Karakaş, S. & Schürmann, M. Are cognitive processes manifested in event-related gamma, alpha, theta and delta oscillations in the EEG? *Neurosci. Lett.* **259**, 165–168 (1999).
126. Başar-Eroglu, C. & Demiralp, T. Event-related theta oscillations: An integrative and comparative approach in the human and animal brain. *Int. J. Psychophysiol.* **39**, 167–195 (2001).
127. Harper, J., Malone, S. M. & Bernat, E. M. Theta and delta band activity explain N2 and P3 ERP component activity in a go/no-go task. *Clin. Neurophysiol.* **125**, 124–132 (2014).
128. Yordanova, J. & Kolev, V. Single-sweep analysis of the theta frequency band during an auditory oddball task. *Psychophysiology* **35**, 116–126 (1998).
129. Trujillo, L. T. & Allen, J. J. B. Theta EEG dynamics of the error-related negativity. *Clin. Neurophysiol.* **118**, 645–668 (2007).
130. Veniero, D. *et al.* Top-down control of visual cortex by the frontal eye fields through oscillatory realignment. *Nat. Commun.* **12**, 1757 (2021).
131. Griffiths, B. J. *et al.* Alpha/beta power decreases track the fidelity of stimulus-specific information. *eLife* **8**, e49562 (2019).

132. Fries, P. Neuronal gamma-band synchronization as a fundamental process in cortical computation. *Annu. Rev. Neurosci.* **32**, 209–224 (2009).
133. Jensen, O., Kaiser, J. & Lachaux, J.-P. Human gamma-frequency oscillations associated with attention and memory. *Trends Neurosci.* **30**, 317–324 (2007).

### Acknowledgements

This paper is part of Pablo Rodríguez-San Esteban's doctoral dissertation at the Doctoral Programme in Psychology of the University of Granada. It was supported by Grants PID2020-119033 GB-I00 (PI Ana B. Chica) and PID2022-141378OB-C22 (PI José A. González-López) funded by MCIN/AEI/10.13039/501100011033 and by “ERDF A way of making Europe”, by the “European Union” or by the “European Union NextGenerationEU/PRTR”. The authors would like to acknowledge Brain Products GmbH for covering the open access publication fees for this article.

### Author contributions

P. R.: Conceptualization; data curation; formal analysis; investigation; methodology; resources; software development; visualisation; writing – original draft; writing – review and editing. J.A.G.: Formal analysis; methodology; software development; data analysis; resources; supervision; writing – review and editing. A. B.C.: Conceptualization; funding acquisition; methodology; project administration; supervision; writing – review and editing.

### Declarations

#### Competing interests

The authors declare no competing interests.

### Additional information

**Supplementary Information** The online version contains supplementary material available at <https://doi.org/10.1038/s41598-025-92490-y>.

**Correspondence** and requests for materials should be addressed to P.R.-S.

**Reprints and permissions information** is available at [www.nature.com/reprints](http://www.nature.com/reprints).

**Publisher's note** Springer Nature remains neutral with regard to jurisdictional claims in published maps and institutional affiliations.

**Open Access** This article is licensed under a Creative Commons Attribution-NonCommercial-NoDerivatives 4.0 International License, which permits any non-commercial use, sharing, distribution and reproduction in any medium or format, as long as you give appropriate credit to the original author(s) and the source, provide a link to the Creative Commons licence, and indicate if you modified the licensed material. You do not have permission under this licence to share adapted material derived from this article or parts of it. The images or other third party material in this article are included in the article's Creative Commons licence, unless indicated otherwise in a credit line to the material. If material is not included in the article's Creative Commons licence and your intended use is not permitted by statutory regulation or exceeds the permitted use, you will need to obtain permission directly from the copyright holder. To view a copy of this licence, visit <http://creativecommons.org/licenses/by-nc-nd/4.0/>.

© The Author(s) 2025